Modeling generation of harmonics in the water window region in hollow core waveguides by mid-infrared femtosecond pulses

A. M. M. Gherman ⓘ ; I. Tóth ✉ ⓘ ; A. G. Ciriolo ⓘ ; R. Martínez Vázquez ⓘ ; A. Nistico ⓘ ; S. Stagira ⓘ ;
V. Toşa ⓘ

Check for updates

Modeling generation of harmonics in the water window region in hollow core waveguides by mid-infrared femtosecond pulses

A. M. M. Gherman,[1] [ID] I. Tóth,[1,a)] [ID] A. G. Ciriolo,[2] [ID] R. Martínez Vázquez,[2] [ID] A. Nistico,[3] [ID] S. Stagira,[3] [ID] and V. Toşa[1] [ID]

AFFILIATIONS

[1]National Institute for R&D of Isotopic and Molecular Technologies, Cluj-Napoca, Romania
[2]Institute for Photonics and Nanotechnologies, National Research Council, Milano, Italy
[3]Physics Department, Politecnico di Milano, Milano, Italy

[a)]Author to whom correspondence should be addressed: istvan.toth@itim-cj.ro

ABSTRACT

We numerically investigate generation of harmonics in the water window region (down to 2.8 nm) by $2\,\mu$m femtosecond pulses propagating in hollow core waveguides filled with high pressure He. Numerical calculations are based on a three dimensional macroscopic model, which solves the pulse propagation by a split-step method, uses the strong field approximation to evaluate the single atom response, and integrates it coherently to obtain the harmonic field. Two configurations for the waveguides are considered: the standard one with a constant diameter of $70\,\mu$m and a conical one with a decreasing diameter from 70 to $50\,\mu$m. We demonstrate that harmonic field enhancement can be obtained in spectral domains of great practical interest, from 2.8 to 20 nm, and identify quasi-phase matching induced by multimode beating as the mechanism responsible for this enhancement.

I. INTRODUCTION

Generation and use of attosecond pulses received recently the full confirmation as a promising field of investigation for future and emerging technologies, being the topic of the Nobel Prize awarded for 2023.[1] Despite the low efficiency, high-order harmonics generation (HHG) in (mainly noble) gases remains the main method to obtain extreme ultraviolet (XUV) or soft X-ray (SXR) attosecond pulses[2] because they can be obtained at large repetition rates and do not need very high laser intensities. Briefly, a femtosecond pulse of infrared or mid-infrared (MIR) wavelength will interact with the target atom or molecule and via the well-known three-step process (electron ionization, acceleration, and recombination) will generate a single or a train of attosecond bursts.[3] The gas medium is traditionally supplied in a jet or in a static cell, but the alternative to use dielectric structures to host the gas and to guide the ultrafast beam is a one way to increase the HHG efficiency and therefore, it is of obvious practical interest. Such structures, in particular, dielectric

hollow core waveguides (HCWs), allow gas confinement at high pressures and keep high laser intensity over longer interaction lengths, leading to a significant chance to increase the HHG yield.[4]

The ways to increase the macroscopic HHG yield are mainly three: (i) to have a driving field intensity high enough and over a large spatial region, such as to induce an intense single atom response and a high-order cutoff, (ii) to have a density of elementary emitters as high as possible, and (iii) to create conditions for phase matching (PM),[5] which is to have constructive interference between the single atomic emission and the harmonic field builtup at a specific point. This last condition is the most important one but difficult to realize because PM usually happens in small spatial regions compared to the whole extension of the medium and in a narrow temporal window compared to the whole extension of the pulse. The higher the photon energy, the shorter the coherence length and the temporal window in which PM happens so many groups tried to find conditions for quasi-phase matching (QPM) by inducing intensity and phase modulation of the driving field by

using modulated waveguides[6–8] or a second counterpropagating field.[9] A distinct approach[10,11] to induce the QPM was to use the driving field intensity variations induced by mode beating along the propagation direction.

An HHG spectrum starts with a few high intensity harmonics, then continues in the plateau of many harmonics of slowly decreasing intensity, and ends abruptly at cut-off harmonics of maximum order $I_p + 3.17U_p$, I_p and U_p being, respectively, the ionization potential of the atom and the ponderomotive energy of an electron in an electromagnetic field $U_p = E^2/4\omega^2$ (in atomic units). To increase the cut-off energy, one needs to increase the laser intensity or the laser wavelength. Power scaling[12] is limited by the level of ionization, which depletes the neutral atom population and, in free space geometries, induces beam defocusing due to the divergent lens created by the free electrons. Using a longer wavelength[13,14] is more promising (provided the MIR source is available) as the cutoff is proportional to the square of the central wavelength λ, although the conversion efficiency of HHG decreases as λ^{-a}, where $5 < a < 6$.[13] In principle, a femtosecond MIR source can generate up to SXR radiation without the need to go to high ionization levels, which can strongly alter the beam intensity and phase.

Attempts to generate coherent radiation in the water window range have been experimentally reported either using optical parameter amplifiers at $1.85 \mu m$ central wavelength and kHz repetition rates[15] or using optical parametric chirped-pulse amplifiers at $2.1 \mu m$[16,17] or $1.6 \mu m$,[18] which can be scaled up in terms of average powers. One of the frequent approaches to increase the HHG flux was to search for conditions in which quasi-phase matching (QPM) of energy or momentum of photons is fulfilled;[8] see a review on this topic.[5] Periodic (sub-millimeter) modulation of the HCW diameter will translate into an intensity modulation of the driving beam and produce harmonic enhancement in the 90 eV[7] or water window[6] regions. As the needed periodic modulations in the HCW become very short, there are technical limitations in achieving further growth of the harmonic cutoff in the SXR regions.

Modeling HHG in HCW complements the experimental efforts, and the tools used for calculating the nonlinear propagation in capillary fibers were recently reviewed by Crego et al.[19] Starting from the standard split-step method,[20,21] time independent or time-dependent models can be built in one dimension or up to three spatial dimensions. The time-dependent models can be further used to calculate the macroscopic response of the medium and then the macroscopic harmonic field built inside the HCW in various configurations. For example, Nurhuda et al.[22] computed the field distribution in a variable pressure setup to avoid or postpone self-focusing, while Jin et al. extended the split-step method to two[23] and three[24] fields of different frequencies to generate a synthesized waveform. A multimode generalized Schrödinger equation[25] was extended to include ionization and plasma effects and, again using the split-step method, was used to calculate the field evolution and the plasma structure[26] inside the capillary.

In the present paper, we explore HHG in an unexplored regime of generation: we assume a 25 fs laser pulse of 2000 nm central wavelength propagating in an 8 mm long HCW filled with 10 bar of He. Two geometries are considered: the standard one with a constant diameter of $70 \mu m$ along the HCW and a conical one with decreasing

diameter from 70 to $50 \mu m$. We show that the conical geometry has promising potential for generating XUV toward SXR attosecond bursts of light, in a spectral region of great interest for applications.

II. MATERIALS AND METHODS

Numerical calculations have been carried out using a 3D non-adiabatic model; see Refs. [27–29] for details, which calculates the macroscopic HHG field in three main steps. First, the propagation equation for the full laser field in the HCW is solved. In an ionized gas, the pulse evolution can be described by the wave equation in a time domain,

$$\nabla^2 E_1(r, z, t) - \frac{1}{c^2}\frac{\partial^2 E_1(r, z, t)}{\partial t^2} = \frac{\omega^2}{c^2}(1 - \eta_{eff}^2)E_1(r, z, t). \quad (1)$$

Here, ω is the central angular frequency of the driving field, while η_{eff} is the space- and time-dependent effective refractive index of the medium,

$$\eta_{eff}(n_a, n_e, r, z, t) = \eta_0(n_a) + \eta_2(n_0)I(r, z, t) - \frac{\omega_p^2(n_e, r, z, t)}{2\omega^2}. \quad (2)$$

As seen in Eq. (2), the refractive index includes three contributions: the first term $\eta_0 = 1 + \delta_1 - i\beta_1$ accounts for the dispersion δ_1 and absorption β_1 and depends linearly on the density of the neutral atoms $n_a(r, z, t) = n_0(z) - n_e(r, z, t)$. The second term contains the intensity-dependent nonlinear refractive index η_2, which represents the optical Kerr-effect. Here, $n_0(z)$ is the total particle density and $I(r, z, t)$ is the instantaneous laser intensity. The last term accounts for plasma defocusing, where $\omega_p(r, z, t)$ is the plasma angular frequency and $n_e(r, z, t)$ is the free electron density calculated from the ionization rates[30] for He. Since ionization is the first step during a laser–atom interaction, the plasma formation is inevitable in the interaction volume, and, in most cases, this last term dominates the fast variation of the medium refractive index. Here, β_1 and δ_1 are computed from atomic form factors for He,[31] while η_2 for He is taken from Ref. [32]. In the range of low photon energies, we used the Sellmeier equation[33] to obtain the refractive index for He and fused silica.

After transforming Eq. (1) in the moving frame (r, z', t'), applying the paraxial approximation, and going to the spectral domain via the Fourier transform, it becomes

$$\nabla_\perp^2 \tilde{E}_1(r, z', \omega) - \frac{2i\omega}{c}\frac{\partial \tilde{E}_1(r, z', \omega)}{\partial z'} = \tilde{G}(r, z', \omega), \quad (3)$$

where

$$\tilde{E}_1(r, z', \omega) = \hat{F}[E_1(r, z', t')]$$

is the Fourier transform of $E_1(r, z', t')$, and

$$\tilde{G}(r, z', \omega) = \hat{F}\left\{\frac{\omega_p^2}{c^2}E_1(r, z', t') - 2\frac{\omega_0^2}{c^2}[\delta_1 + \eta_2 I(r, z', t')]E_1(r, z', t')\right\}$$

$$(4)$$

is the Fourier transform of the free term.

The model was first developed for free space;[27–29] however, for propagation in the HCW, we used the split-step method. The first step solves the homogeneous part of Eq. (3) by advancing one step each spectral component along the propagation direction while assuming the field as a superposition of EH_{1m} eigenmodes to satisfy the boundary conditions in the hollow dielectric waveguide[34] for a linearly polarized field. For a detailed description of this procedure, see Ref. 23.

The second step solves Eq. (3) with the free term included but without the diffraction term, that is, a first order differential equation. Since the free term contains the solution itself, we apply here an iterative procedure as follows: (i) the field $E_1(r, z', \omega)$ is Fourier transformed to obtain $E_1(r, z', t)$, (ii) recalculate the free term in the time domain, then use Eq. (4) to obtain $\tilde{G}(r, z', \omega)$, and (iii) solves the first order differential equation over the same dz step and obtain a new $E_1(r, z', \omega)$; repeat steps from (i) to (iii) until the difference between two successive solutions is below a specified threshold. The number of iterations depends on the propagation conditions, such as pressure, ionization fraction, gas nature, etc., but usually is more than two, which proves the necessity of the iterations.

The solution $E_1(r, z, t)$ is then used to calculate the gas polarization $P_{nl}(r, z, t)$ in the strong field approximation[35] over the whole interaction region. A single dipole response to the field, $d_{nl}(r, z, t)$, was obtained computing the Lewenstein integral,[35] and this is the most time consuming part of the model. Macroscopic polarization $P_{nl}(r, z, t) = (n_0(z) - n_e(r, z, t))d_{nl}(r, z, t)$ was used to solve the propagation equation for the harmonic field $E_h(r, z, t)$,

$$\nabla^2 E_h(r, z, t) - \frac{\eta^2}{c^2}\frac{\partial^2 E_h(r, z, t)}{\partial t^2} = \frac{\partial^2 P_{nl}(r, z, t)}{\partial t^2}, \quad (5)$$

which have the same form as Eq. (1), but having atomic polarization as a source. This equation was solved with the method developed[29] for the free space, because the single atom polarization is closely confined around the HCW axis and practically does not interact with guide walls. Our previous reports of modeling experimental data[4,36] demonstrate that this assumption is a valid one. In this equation, the refractive index η takes into account the atom dispersion and absorption but ignores free electron dispersion because the plasma frequency is much lower than the frequencies of high-order harmonics.

For the parameters used in building the model, we set a spatial grid of 400/250 nodes in axial/radial directions and a temporal domain of 128 optical cycles, each cycle having 2048 points, as the full electric field needs to be described. A full runtime depends on the machine used, being in the range of a few hours.

III. RESULTS

The main result of the propagation model is the electric field $E_1(r, z, t)$ or equivalently $E_1(r, z, \omega)$ inside the HCW, but additional results include (r, z) maps of the peak intensity and phase of the electric field and also maps of the electron density and the refractive index resulted after propagation. Other quantities, such as pulse energy, mode energies, mode amplitudes as well as spectral characteristics of the field, can also be extracted from the calculation.

The HHG model yields the harmonic field $E_H(r, z, \omega)$ inside the HCW and other useful quantities, such as the total harmonic

power generated at a specific frequency, a total power spectrum at exit or at user specified axial positions, spatial maps of the single atom polarizations and macroscopic harmonic fields, as well as far field reaching a specific position relevant for the experiment.

The model allows for a variety of beam profiles at the injection plane (Gaussian, truncated Gaussian, Bessel, etc.) as well as for an arbitrary pressure profile along the z direction. The initial field can be specified in time or in a frequency domain. The layout of the model was designed closely connected to the experimental configuration used in Refs. 4 and 37 assuming the same HCW architecture, but different values for the pulse energy and duration, central wavelength, focusing geometry, gas pressure, and HCW size, which will be detailed later.

A. Testing the propagation model

Testing the model against experimental data was a necessary step in the model development. Here, we have to mention that a very good agreement was found between experimental data reporting dependence along the propagation direction of Ar fluorescence[38] and the total electron density obtained from simulations.[39]

Successful tests[39] were also performed against results obtained from solving the Schrödinger equation for pulse propagation in the HCW.[26] In addition, we used two different methods to validate the split-step method: one solving the propagation equation in the time domain by finite differences and the other using normal mode decomposition in the frequency domain to solve Maxwell's equations. Both methods are available in Lumerical software,[40] and in this framework, we built a three dimensional model for pulse propagation in a straight HCW in vacuum. The Gaussian profile obeying the optimal coupling condition for the beam size was assumed at an injection plane. We have to mention that, for reasons of memory and run-time limitations, the Lumerical calculations were performed only on a smaller size HCW. While with a split-step method we solved the propagation in a HCW having length $L = 8$ mm and diameter
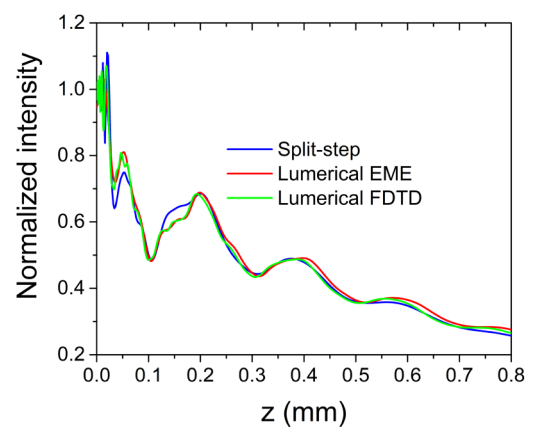

FIG. 1. On-axis normalized intensity calculated for a HCW with the split-step method described in Sec II and with two Ansys Lumerical modules: Eigen Mode Expansion (EME) and Finite Difference Time Domain (FDTD).

$D = 70\,\mu m$, with Lumerical models, the waveguide was scaled down to $L/10$ in length and $D/\sqrt{10}$ in diameter. In the end, split-step results were also adjusted to take into account the different attenuation factors[34] in the two waveguides. The results are given in Fig. 1, and as one can see, the agreement between the Lumerical results and the split-step method was satisfactory.

Simulation results of the model for HHG conditions close to specific experimental situations using 800 nm pulses and a pressure profile similar to the one used here[4,37] or in a multijet configuration[36] were reported earlier.

B. Influence of the initial beam profile at an injection plane

The large majority of the results reported in the literature[23,24] are obtained assuming that the initial profile of the field at the entrance of the HCW (with a radius a) is a Bessel profile, because the Gaussian having the waist at an optimal coupling value, $w = 2a/\pi$, is very close to the $J_0(r/a)$ profile. However, we found out that the propagation along the HCW is noticeably dependent on the choice of the initial profile. The difference comes from the modal decomposition of the two profiles. While the Bessel profile contains only the fundamental mode EH_{11}, the Gauss profile decomposition contains also higher order modes. Although the amplitudes of these modes are small compared to fundamental, the beating of these modes produces oscillations of the total field during propagation. In Fig. 1, these oscillations are clearly present, regardless of the method used to calculate the field.

The mode beating for a 25 fs pulse at 2000 nm central wavelength can be seen in Fig. 2(a), where for three different plateau pressures, we show the on-axis peak intensities along 8 mm in the HCW of constant $70\,\mu m$ diameter. The pressure profile was calculated[4] in an OpenFoam[41] model taking into account the injection and exit holes for the gas in the HCW. As one can note, the mode beating survives at all pressures and maintains the positions of minima and maxima at different pressures; however, the intensity for 10 bar peak pressure drops more with the propagation distance. The pulse energy loss is also dependent on pressure being around 30% for 1 bar and 50% for 10 bar peak pressure. Figure 2(b) shows the energies of the three lowest order modes, which confirm the

transfer of energy between the modes and produce oscillations of the total field intensity via mode beating. Seen in Fig. 2(c) are the radial profiles of the driving field intensity for a few z positions, including the HCW exit. The deviations from a Gaussian profile are obvious, but due to the low ionization fraction, the profiles preserve a high intensity close to the axis and decrease continuously toward the HCW walls. The radial profiles for a few harmonics at the HCW exit are also shown, confirming the HHG in a region well confined around the guide axis.

On the other hand, the Bessel initial profile will yield a much smoother intensity profile in the guide and a different phase of the driving field, and this will produce different HHG conditions in terms of a single atom response and phase matching. Therefore, from the point of view of achieving a realistic description of the HHG process, the choice of the initial radial profile as close as possible to the experiment is very important, although it looks a rather technical detail.

C. Beam propagation in modulated HCW

One can build a large variety of HCW as well as various configurations[37] for the gas flow. The combination of these parameters can lead to a variety of driving field intensity and pressure profiles, which will govern the efficiency of the HHG process and the spectral composition of the attosecond pulse trains. One of the structures that is proposed here for an HHG experiment is the HCW with a variable diameter. In such a structure, the mode beating has a variable period; therefore, in principle, one could control the evolution of the laser intensity and phase in order to optimize the HHG yield.

We consider in the following two cases of cylindrical and conical shapes, the first one with a constant diameter of $70\,\mu m$, the second having a linearly variable diameter starting from $70\,\mu m$ at a beam input and ending after 8 mm with a diameter of $50\,\mu m$. A pulse of 25 fs duration, 0.15 mJ energy, and 2000 nm central wavelength propagates in the He gas at 10 bar peak pressure. The input peak intensity depends on the initial waveguide diameter as we imposed best coupling in each case.

The on-axis peak intensities along the waveguide are shown in Fig. 3(a) for the two cases. These peak intensities are one order of magnitude higher than the damage threshold[42] for fused silica,
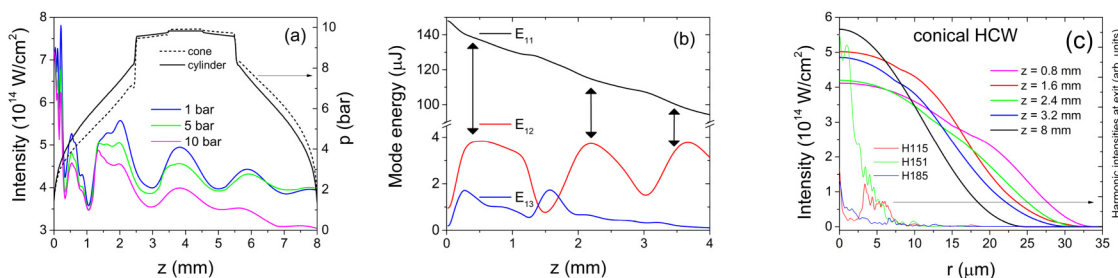
FIG. 2. (a) On-axis peak intensities in the cylindrical HCW and for three different pressures. The 10 bar pressure profiles for both cylindrical and conical HCW are also shown. (b) Mode energies of the first three lowest order modes; the arrows indicate the region where the energy transfer between the first two normal modes takes place. (c) Radial dependence of the driving field intensity (left axis) after a few propagation distances indicated in the legend. The distortion of the profile is due to the higher order mode contributions to the total field. Radial profiles at exit for a few harmonics (right axis) are also shown.
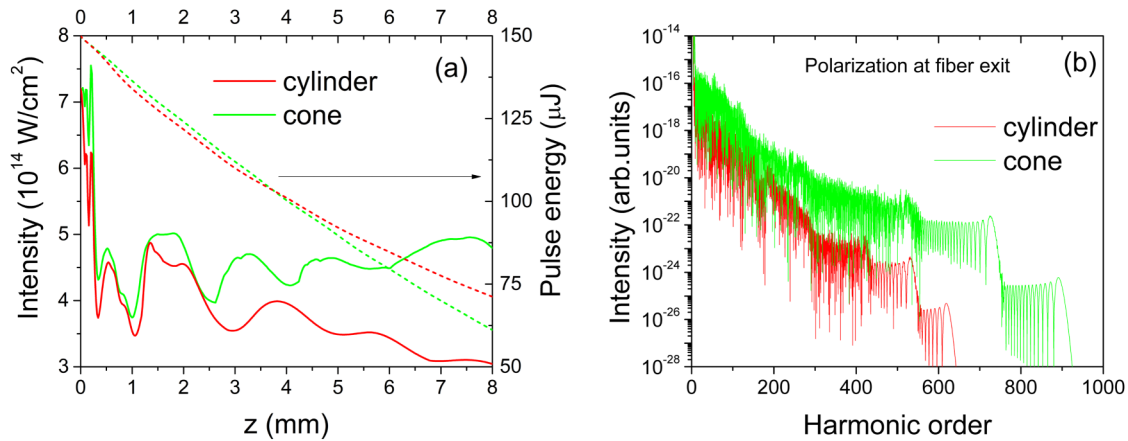
FIG. 3. (a) On-axis peak intensity along the propagation distance for cylindrical and conical waveguides as specified in the legend. The pulse energy evolution is also shown. (b) Single atom polarization at a fiber exit for the two waveguides.

which is approximately 10^{13} W/cm². Under optimal launch alignment conditions, the proposed guiding structures are capable of handling these energy densities without being damaged. Indeed, the main characteristic of hollow core waveguides is that the light is confined to an air core rather than in a solid material, thus allowing to work with extremely high laser peak energies, even some order of magnitude higher than the damage threshold.[43] The thermal load due to radiative losses along the waveguide constitutes a second source of damage, and overheating of the fused silica substrate might degrade the device; thus, active cooling systems are experimentally used to mitigate this effect, such as water cooling.[44]

The intensities shown in Fig. 3(a) demonstrate that by changing the HCW diameter, one can modify the evolution of the intensity (and phase, not shown here) inside the HCW. As we see here, one can prevent the decrease of the peak intensity in the second part of the waveguide (due to propagation losses) by using the conical convergent waveguide. The most important gain though is the single atom polarization. This is shown in Fig. 3(b) for the on-axis fiber exit, and one can see that both the cutoff and the yield are enhanced in the conical geometry, and this holds for the last 5 mm of propagation where the intensity of the conical waveguide departs from that of the cylindrical one. One can also note multiple cutoffs in the polarization spectra, generated in different half-cycles of the driving pulse. For the conical case, these multiple cutoffs fall in the spectral region where an enhancement was observed, as we will see in the following.

The harmonic spectra built in the two types of waveguides are shown in Fig. 4, where we represent the yield as an emission power,

$$Y(q, z_f) = 2\pi \int_0^a E_h^2(r, z_f, q)r\,dr, \quad (6)$$

in the near field at fiber exit $z_f = 8$ mm. The most striking feature of the spectrum for the conical HCW is the yield at very high orders, amplified in a very large order range (from 450 to 700),

which corresponds to photon wavelengths in the range from 2.85 to 4.5 nm. The spectrum shows a cutoff around harmonic order 700, which corresponds to about 430 eV, which is in the water window and also above the nitrogen K-edge (410 eV). Two other interesting spectral ranges show yield enhancement of the power: one around 7.6 nm and the other in the 11–13 nm range. The power spectrum generated in the cylindrical HCW shows less enhancement at very high orders but a higher yield below order 100 (20 nm).

D. Quasi-phase-matching in HCW

In the following, we will analyze finer details of the HHG process for the cylindrical and conical geometries. Shown in Fig. 5 is the dependence on the propagation distance of the emission power $Y(q, z)$ and atomic polarization at 3.75 nm photon
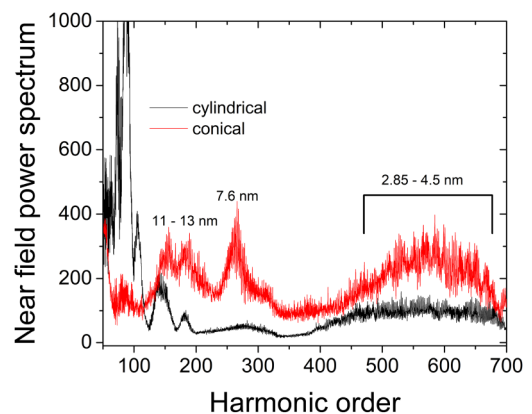
FIG. 4. Harmonic near field at 8 mm, built-up in the conical and cylindrical HCW. The spectral regions with field enhancement are also mentioned in terms of wavelengths.

23 July 2024 09:56:54
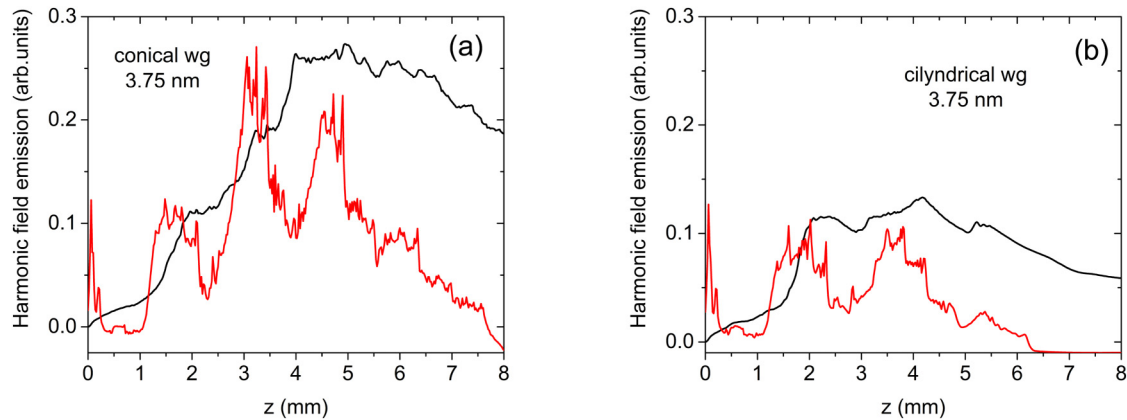
FIG. 5. Evolution along the HCW of the total emission power (black) and atomic polarization (red) for a harmonic frequency of order $q = 531$. Conical (a) and cylindrical (b) configurations are shown. The vertical axis scale is in arbitrary units but the same in both panels.

wavelength ($q = 531$) for the conical (a) and cylindrical (b) geometries. Here, the emission power is the integral [Eq. (6)] calculated over the cross section of the guide and for all grid points of the axial direction, while atomic polarization is an average of the polarization along the radial direction. One can see that the atomic polarization has strong variations along the propagation direction, and the emission power shows a steady increase in the first 5 mm and then a continuous decrease for the next 3 mm. However, in both cases, we see regions where atomic polarization has strong yields, alternating with regions with weak signals. This is due to mode beating inside the HCW, which produces regions of high driving intensities followed by regions of low intensity and low ionization, thus low polarization signals. In fact, the oscillations that we see in the driving field intensities in Fig. 3(a) (with maxima around 1.5, 3, and 4.5 mm) are also observed in the variations of the polarization with maxima of yield in the same positions. This is clearly seen in Fig. 5(a) for the conical case, while for the cylindrical geometry [Fig. 5(b)], we observe only two regions with intense polarization and a steady decrease after. In the last 3 mm, the atomic polarization for both cases is weaker and does not contribute anymore to the increase of the total harmonic field.

The alternation of regions of strong and weak sources for harmonics has been identified[10,11] as having potential for inducing a QPM regime of HHG. In Ref. 11, the propagation of the driving field was solved only for vacuum and the harmonic buildup was obtained using a 1D code under optimal matching conditions for the normalized harmonic source terms. Here, both driving field and harmonic field were calculated in a 3D geometry assuming an axial symmetry of the problem and phase matching at a microscopic level dictated by the phases of the single atom response and the total harmonic field. Our results also suggest a QPM regime of a harmonic buildup. The evolution of the emission power in Fig. 5(a), having regions of a strong increase (corresponding to a high yield of polarization) alternating with regions of almost no increase (where polarization is weak). For the cylindrical case, the decrease of the peak intensity of the driving field is dominant over

the beating oscillations so that we only see the first jump in the harmonic intensity.

In Fig. 6, we present the results of a similar analysis for two lower order harmonics at 7.6 nm ($q = 263$) and 5.5 nm ($q = 361$), which in the power spectrum at a conical HCW exit (Fig. 4) show a local narrow maximum and, respectively, a minimum of emission. As the scale is the same as in Fig. 5, one can see that the atomic polarization is more than two orders of magnitude higher because we have lower orders, but the emission power evolution does not follow anymore the maxima of the single atom polarization. Here, we have two examples in which the coherence length of the QPM fit only partially (for $q = 263$) or does not fit (for $q = 361$) with the spacing between two successive maxima for the polarization. In Fig. 6(a), the total emission shows a first maximum corresponding to the first polarization maximum and a second revival as it overlaps partially with the second polarization maximum. For $q = 361$ [Fig. 6(b)], the total emission shows only a region of enhancement corresponding to the first maximum of polarization while is clearly not sensitive to its second maximum, as it is also the case in Fig. 6(a) at the third polarization maximum.

The picture coming out from these results (Figs. 5 and 6) is that the spatial distribution of the single atom polarization for a specific range of frequencies is in close dependence on the spatial distribution of the laser field intensity, which in turn is governed by the mode beating inside the HCW. The pressure or better the distribution of pressure influences the strength of the polarization but less the driving field intensity. When quasi-phase matching coherence length equals the pace in which polarization varies, we see the increase in the total harmonic field (Fig. 5); otherwise, this condition can be partially fulfilled [Fig. 6(a)] or not fulfilled [Fig. 6(b)]. While polarization has almost constant periodicity in space, QPM coherence length decreases during propagation so that the QPM condition deteriorates. This can be seen in all cases so that toward the exit from the guide, the harmonic yield decreases, also because of the decrease of the pressure, absorption playing a minor role for high-order harmonics.
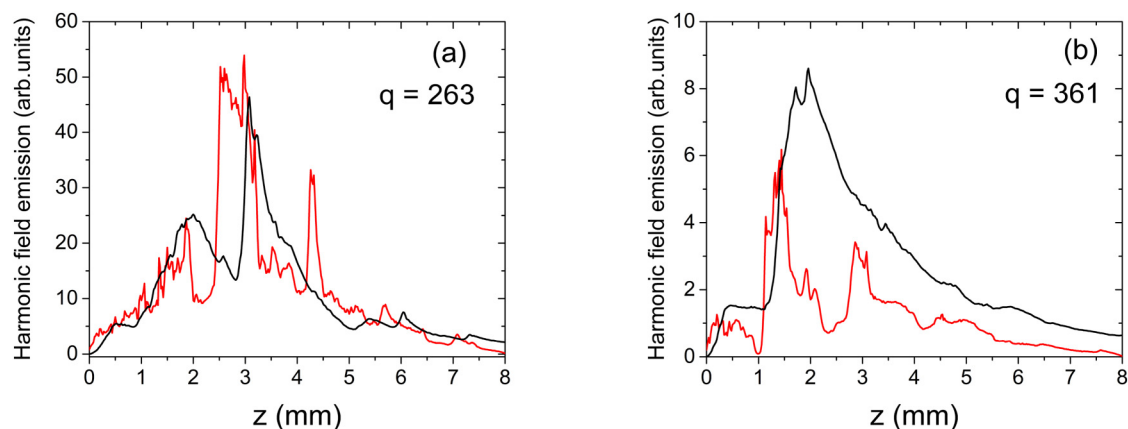
FIG. 6. Evolution along the conical HCW of the total emission power (black) and atomic polarization (red) for harmonic frequencies of order $q = 263$ (a) and $q = 361$ (b). Same units as in Fig. 5 for the vertical axes.

An interesting issue is HHG at the high pressures[45] we assumed in the calculations. For such a high pressure, the probability of exciting neighboring atoms by laser-released high-energy electrons is not negligible and has to be considered. Experiments[46,47] at driving field intensities around 5×10^{15} W/cm^2 and in high densities, gas jets evidenced the presence of different excitation mechanisms that are contributing in different ratios to the overall x-ray emission yields. At these high intensities, direct HHG emission competes with indirect collisions with neighboring atoms by electrons having "drifted away" from the original parent ion. However, HHG experiments performed at one order of magnitude lower intensity and 3.9 μm driving wavelength[48] found that the optimum pressure for an HHG yield is around 35 atm. This supports the assumption that at lower intensities, perturbation of the electron trajectories from the neighboring atoms is rather a source of decoherence, without affecting too much the single dipole amplitude and phase and consequently the phase matching process.

IV. CONCLUSIONS

In the present work, we studied the generation of a high-order harmonic by mid-infrared femtosecond laser pulses in a high pressure helium gas sample, confined inside cylindrical or conical hollow waveguides. The reduction of the waveguide radius along the propagation, like in the conical configuration, results to improve the generation process in terms of a spectral distribution and emission power. Interestingly, it also shows enhanced emission of wavelength photons under 14 nm. This buildup of the harmonic field in the water window region is due to quasi-phase matching induced by the oscillations of the single atom polarization, which in turn originates from driving field intensity variations due to mode beating inside the hollow core waveguide.

From an experimental point of view, these hollow waveguide structures could be easily produced by laser micromachining techniques as previously demonstrated.[37] Technical challenges, such as implementation of the vacuum system for high gas pressures or elimination of the thermal load due to radiative losses along the waveguide, are still to be solved. The perspective of compact and efficient laser sources in the extreme ultraviolet region will be of great impact in fields, such as XUV metrology and photolithography, which presently rely either on large synchrotron facilities[49] or bulk, low efficiency, plasma based sources.[50]

AUTHOR DECLARATIONS
Conflict of Interest

The authors have no conflicts to disclose.

Author Contributions

A. M. M. Gherman: Data curation (equal); Methodology (lead); Validation (lead); Writing – original draft (equal); Writing – review & editing (equal). **I. Tóth:** Investigation (equal); Software (equal); Visualization (equal); Writing – original draft (equal); Writing – review & editing (equal). **A. G. Ciriolo:** Data curation (equal); Formal analysis (equal); Investigation (equal); Writing – review & editing (equal). **R. Martínez Vázquez:** Formal analysis (equal); Methodology (equal); Validation (equal); Writing – review & editing (equal). **A. Nistico:** Data curation (equal); Investigation (equal); Writing – review & editing (equal). **S. Stagira:** Funding acquisition (lead); Methodology (equal); Project administration (lead); Resources (equal); Supervision (equal); Writing – review & editing (equal). **V. Toşa:** Conceptualization (lead); Data curation (equal); Investigation (equal); Methodology (equal); Software (equal); Supervision (equal); Validation (equal); Writing – original draft (lead); Writing – review & editing (equal).

DATA AVAILABILITY

The data that support the findings of this study are available from the corresponding author upon reasonable request.

REFERENCES

[1] "The Nobel Prize in Physics 2023," Nobel Prize outreach; see https://www.nobelprize.org/prizes/physics/2023/summary/; accessed 28 February 2024.

[2] F. Krausz and M. Ivanov, "Attosecond physics," Rev. Mod. Phys. **81**, 163–234 (2009).

[3] K. Midorikawa, "Progress on table-top isolated attosecond light sources," Nat. Photonics **16**, 267–278 (2022).

[4] A. G. Ciriolo, R. M. Vázquez, V. Tosa, A. Frezzotti, G. Crippa, M. Devetta, D. Faccialá, F. Frassetto, L. Poletto, A. Pusala, C. Vozzi, R. Osellame, and S. Stagira, "High-order harmonic generation in a microfluidic glass device," J. Phys.: Photonics **2**, 024005 (2020).

[5] L. Hareli, G. Shoulga, and A. Bahabad, "Phase matching and quasi-phase matching of high-order harmonic generation—A tutorial," J. Phys. B: At. Mol. Opt. Phys. **53**, 233001 (2020).

[6] E. Gibson, A. Paul, N. Wagner, R. Tobey, D. Gaudiosi, S. Backus, I. Christov, A. Aquila, E. Gullikson, D. Attwood, M. Murnane, and H. Kapteyn, "Coherent soft x-ray generation in the water window with quasi-phase matching," Science **302**, 95–98 (2003).

[7] A. Paul, R. Bartels, R. Tobey, H. Green, S. Weiman, I. Christov, M. Murnane, H. Kapteyn, and S. Backus, "Quasi-phase-matched generation of coherent extreme-ultraviolet light," Nature **421**, 51–54 (2003).

[8] A. Bahabad, M. M. Murnane, and H. C. Kapteyn, "Quasi-phase-matching of momentum and energy in nonlinear optical processes," Nat. Photonics **4**, 570–575 (2010).

[9] A. L. Lytle, X. Zhang, R. L. Sandberg, O. Cohen, H. C. Kapteyn, and M. M. Murnane, "Quasi-phase matching and characterization of high-order harmonic generation in hollow waveguides using counterpropagating light," Opt. Express **16**, 6544–6566 (2008).

[10] M. Zepf, B. Dromey, M. Landreman, P. Foster, and S. M. Hooker, "Bright quasi-phase-matched soft-x-ray harmonic radiation from argon ions," Phys. Rev. Lett. **99**, 143901 (2007).

[11] B. Dromey, M. Zepf, M. Landreman, and S. M. Hooker, "Quasi-phasematching of harmonic generation via multimode beating in waveguides," Opt. Express **15**, 7894–7900 (2007).

[12] C. M. Heyl, C. L. Arnold, A. Couairon, and A. L'Huillier, "Introduction to macroscopic power scaling principles for high-order harmonic generation," J. Phys. B: At. Mol. Opt. Phys. **50**, 013001 (2016).

[13] P. Colosimo, G. Doumy, C. I. Blaga, J. Wheeler, C. Hauri, F. Catoire, J. Tate, R. Chirla, A. M. March, G. G. Paulus, H. G. Muller, P. Agostini, and L. F. DiMauro, "Scaling strong-field interactions towards the classical limit," Nat. Phys. **4**, 386–389 (2008).

[14] A. S. Emelina, M. Y. Emelin, and M. Y. Ryabikin, "Wavelength scaling laws for high-order harmonic yield from atoms driven by mid- and long-wave infrared laser fields," J. Opt. Soc. Am. B **36**, 3236–3245 (2019).

[15] S. L. Cousin, F. Silva, S. Teichmann, M. Hemmer, B. Buades, and J. Biegert, "High-flux table-top soft x-ray source driven by sub-2-cycle, CEP stable, 1.85-μm 1-kHz pulses for carbon K-edge spectroscopy," Opt. Lett. **39**, 5383–5386 (2014).

[16] G. J. Stein, P. D. Keathley, P. Krogen, H. Liang, J. P. Siqueira, C.-L. Chang, C.-J. Lai, K.-H. Hong, G. M. Laurent, and F. X. Kärtner, "Water-window soft x-ray high-harmonic generation up to the nitrogen K-edge driven by a kHz, 2.1 μm OPCPA source," J. Phys. B: At. Mol. Opt. Phys. **49**, 155601 (2016).

[17] G. Marcus, W. Helml, X. Gu, Y. Deng, R. Hartmann, T. Kobayashi, L. Strueder, R. Kienberger, and F. Krausz, "Subfemtosecond k-shell excitation with a few-cycle infrared laser field," Phys. Rev. Lett. **108**, 023201 (2012).

[18] N. Ishii, K. Kaneshima, K. Kitano, T. Kanai, S. Watanabe, and J. Itatani, "Carrier-envelope phase-dependent high harmonic generation in the water window using few-cycle infrared pulses," Nat. Commun. **5**, 3331 (2014).

[19] A. Crego, J. S. Roman, and E. C. Jarque, "Tools for numerical modelling of nonlinear propagation in hollow capillary fibres and their application," J. Opt. **25**, 024005 (2023).

[20] G. P. Agrawal, *Nonlinear Fiber Optics* (Academic Press, Elsevier, Inc., Burlington, MA, 2007).

[21] R. Deiterding and S. W. Poole, "Robust split-step Fourier methods for simulating the propagation of ultra-short pulses in single- and two-mode optical communication fibers," arXiv:1504.01331v1 (2015).

[22] M. Nurhuda, A. Suda, K. Midorikawa, and H. Budiono, "Control of self-phase modulation and plasma-induced blueshifting of high-energy, ultrashort laser pulses in an argon-filled hollow fiber using conjugate pressure-gradient method," J. Opt. Soc. Am. B **22**, 1757–1762 (2005).

[23] C. Jin, K.-H. Hong, and C. D. Lin, "Optimal generation of spatially coherent soft x-ray isolated attosecond pulses in a gas-filled waveguide using two-color synthesized laser pulses," Sci. Rep. **6**, 38165 (2016).

[24] B. Li, X. Tang, K. Wang, C. Zhang, Z. Guan, B. Wang, C. D. Lin, and C. Jin, "Generation of intense low-divergence isolated soft-x-ray attosecond pulses in a gas-filled waveguide using three-color synthesized laser pulses," Phys. Rev. Appl. **18**, 034048 (2022).

[25] F. Poletti and P. Horak, "Description of ultrashort pulse propagation in multimode optical fibers," J. Opt. Soc. Am. B **25**, 1645–1654 (2008).

[26] R. T. Chapman, T. J. Butcher, P. Horak, F. Poletti, J. G. Frey, and W. S. Brocklesby, "Modal effects on pump-pulse propagation in an Ar-filled capillary," Opt. Express **18**, 13279–13284 (2010).

[27] V. Tosa, E. Takahashi, Y. Nabekawa, and K. Midorikawa, "Generation of high-order harmonics in a self-guided beam," Phys. Rev. A **67**, 063817 (2003).

[28] V. Tosa, H. T. Kim, I. J. Kim, and C. H. Nam, "High-order harmonic generation by chirped and self-guided femtosecond laser pulses. II. Time-frequency analysis," Phys. Rev. A **71**, 063808 (2005).

[29] V. Tosa, K. T. Kim, and C. H. Nam, "Macroscopic generation of attosecond-pulse trains in strongly ionized media," Phys. Rev. A **79**, 043828 (2009).

[30] A. Scrinzi, M. Geissler, and T. Brabec, "Ionization above the Coulomb barrier," Phys. Rev. Lett. **83**, 706–709 (1999).

[31] C. T. Chantler, "Detailed tabulation of atomic form factors, photoelectric absorption and scattering cross section, and mass attenuation coefficients in the vicinity of absorption edges in the soft x-ray (Z=30–36, Z=60–89, E=0.1 keV–10 keV), addressing convergence issues of earlier work," J. Phys. Chem. Ref. Data **29**, 597–1056 (2000).

[32] X. F. Li, A. L'Huillier, M. Ferray, L. A. Lompré, and G. Mainfray, "Multiple-harmonic generation in rare gases at high laser intensity," Phys. Rev. A **39**, 5751–5761 (1989).

[33] M. N. Polyanskiy, "Refractiveindex.info database of optical constants," Sci. Data **11**, 94 (2024).

[34] E. A. J. Marcatili and R. A. Schmeltzer, "Hollow metallic and dielectric waveguides for long distance optical transmission and lasers," Bell Syst. Tech. J. **43**, 1783–1809 (1964).

[35] M. Lewenstein, P. Balcou, M. Y. Ivanov, A. L'Huillier, and P. B. Corkum, "Theory of high-harmonic generation by low-frequency laser fields," Phys. Rev. A **49**, 2117–2132 (1994).

[36] A. G. Ciriolo, R. Martínez Vázquez, G. Crippa, M. Devetta, D. Faccialà, P. Barbato, F. Frassetto, M. Negro, F. Bariselli, L. Poletto, V. Tosa, A. Frezzotti, C. Vozzi, R. Osellame, and S. Stagira, "Microfluidic devices for quasi-phase-matching in high-order harmonic generation," APL Photonics **7**, 110801 (2022).

[37] R. Martínez Vázquez, A. G. Ciriolo, G. Crippa, V. Tosa, F. Sala, M. Devetta, C. Vozzi, S. Stagira, and R. Osellame, "Femtosecond laser micromachining of integrated glass devices for high-order harmonic generation," Int. J. Appl. Glass Sci. **13**, 162–170 (2022).

[38] C. A. Froud, R. T. Chapman, E. T. F. Rogers, M. Praeger, B. Mills, J. Grant-Jacob, T. J. Butcher, S. L. Stebbings, A. M. de Paula, J. G. Frey, and

23 July 2024 09:56:54

W. S. Brocklesby, "Spatially resolved Ar* and Ar+* imaging as a diagnostic for capillary-based high harmonic generation," J. Opt. A: Pure Appl. Opt. **11**, 054011 (2009).

[39]V. Tosa, A. G. Ciriolo, R. M. Vazquez, C. Vozzi, and S. Stagira, "Modeling femtosecond pulse propagation and high harmonics generation in hollow core fibers," in *EPJ Web of Conferences* (EDP Sciences, 2021), Vol. 255; see https://doi.org/10.1051/epjconf/202125511005.

[40]Ansys Lumerical, Inc., see https://www.ansys.com/products/optics (2022).

[41]The OpenFoam Foundation, see https://openfoam.org/ (2024).

[42]B. Chimier, O. Utéza, N. Sanner, M. Sentis, T. Itina, P. Lassonde, F. Légaré, F. Vidal, and J. C. Kieffer, "Damage and ablation thresholds of fused-silica in femtosecond regime," Phys. Rev. B **84**, 094104 (2011).

[43]Q. Ran, L. Wang, L. Li, H. Li, Q. Wang, and Y. Zhang, "Coupling of subterawatt laser into hollow core waveguide for high-harmonic generation above 200 eV," IEEE Photonics Technol. Lett. **32**, 1393–1396 (2020).

[44]Z. Filus, P. Ye, T. Csizmadia, T. Grósz, L. Gulyás Oldal, M. De Marco, M. Füle, S. Kahaly, K. Varjú, and B. Major, "Liquid-cooled modular gas cell system for high-order harmonic generation using high average power laser systems," Rev. Sci. Instrum. **93**, 073002 (2022).

[45]"We thank one of the referees for drawing out our attention on this issue."

[46]Y. Deng, Z. Zeng, Z. Jia, P. Komm, Y. Zheng, X. Ge, R. Li, and G. Marcus, "Ultrafast excitation of an inner-shell electron by laser-induced electron recollision," Phys. Rev. Lett. **116**, 073901 (2016).

[47]Y. Deng, Z. Zeng, P. Komm, Y. Zheng, W. Helml, X. Xie, Z. Filus, M. Dumergue, R. Flender, M. Kurucz, L. Haizer, B. Kiss, S. Kahaly, R. Li, and G. Marcus, "Laser-induced inner-shell excitations through direct electron re-collision versus indirect collision," Opt. Express **28**, 23251–23265 (2020).

[48]T. Popmintchev, M.-C. Chen, D. Popmintchev, P. Arpin, S. Brown, S. Ališauskas, G. Andriukaitis, T. Balčiunas, O. D. Mücke, A. Pugzlys, A. Baltuška, B. Shim, S. E. Schrauth, A. Gaeta, C. Hernández-García, L. Plaja, A. Becker, A. Jaron-Becker, M. M. Murnane, and H. C. Kapteyn, "Bright coherent ultrahigh harmonics in the keV x-ray regime from mid-infrared femtosecond lasers," Science **336**, 1287–1291 (2012).

[49]B. Jiang, C. Feng, C. Li, Z. Bai, W. Wan, D. Xiang, Q. Gu, K. Wang, Q. Zhang, D. Huang, and S. Chen, "A synchrotron-based kilowatt-level radiation source for EUV lithography," Sci. Rep. **12**, 3325 (2022).

[50]D.-K. Yang, D. Wang, Q.-S. Huang, Y. Song, J. Wu, W.-X. Li, Z.-S. Wang, X.-H. Tang, H.-X. Xu, S. Liu, and C.-Q. Gui, "The development of laser-produced plasma EUV light source," Chip **1**, 100019 (2022).

23 July 2024 09:56:54